Published in final edited form as:
J Phys Chem B. 2020 December 31; 124(52): 11835–11842. doi:10.1021/acs.jpcb.0c09498.

Stark Spectroscopy of Lumichrome: A Possible Candidate for Stand-Off Detection of Bacterial Quorum Sensing

Cornelius van Galen,
Department of Chemistry, Temple University, Philadelphia, Pennsylvania 19122, United States

David T. Barnard,
Department of Chemistry, Temple University, Philadelphia, Pennsylvania 19122, United States

Robert J. Stanley
Department of Chemistry, Temple University, Philadelphia, Pennsylvania 19122, United States

Abstract

Lumichrome (7,8-dimethylalloxazine, LC) is a natural photodegradation product and catabolite of flavin coenzymes. Although not a coenzyme itself, LC is used for biosignaling in plants and single-celled organisms, including quorum sensing in the formation of biofilms. The noninvasive detection of in vivo lumichrome would be useful for monitoring this signaling event. For molecules that undergo significant charge redistribution upon light excitation (e.g., intramolecular charge transfer), there are optical detection methods (e.g., second-harmonic generation) that would be well suited to this task. Here, we have used Stark spectroscopy to measure the extent and direction of charge redistribution in photoexcited LC. Stark and low-temperature absorption spectra were obtained at 77 K on LC in ethanol glasses and analyzed using the Liptay analysis to obtain the difference dipole moments and polarizabilities. These data were complemented by a computational analysis of the excited states using density functional theory (DFT) at the TD-B3LYP/6–311+G(2d,p) level of theory.

Graphical Abstract

Corresponding Author: Robert J. Stanley – *Department of Chemistry, Temple University, Philadelphia, Pennsylvania 19122, United States*; rstanley@temple.edu.

Supporting Information
The Supporting Information is available free of charge at https://pubs.acs.org/doi/10.1021/acs.jpcb.0c09498.
LC and LF geometry and orientations, tabulated and diagrammatic difference and transition dipole vector components; molecular geometry of lumichrome and lumiflavin optimized in the gas phase at the B3LYP/6–311+G(2d,p) level of theory using Gaussian16; first 10 excited states of gas phase lumichrome and lumiflavin calculated at the B3LYP/6–311+G(2d,p) level of theory using Gaussian16 (PDF)

Complete contact information is available at: https://pubs.acs.org/10.1021/acs.jpcb.0c09498

The authors declare no competing financial interest.

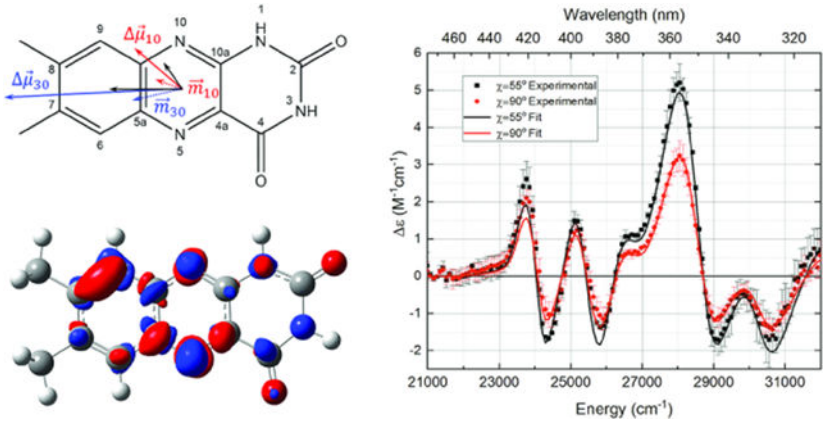

INTRODUCTION

Lumichrome (7,8-dimethyl-1*H*-benzo[*g*]pteridine-2,4-dione or LC) is a tautomer of flavin (7,8-dimethylbenzo[*g*]pteridine-2,4(3*H*,10*H*)-dione or 7,8-dimethylisoalloxazine or FL) in which the N10 hydrogen shifts to the N1 atom with a resultant decrease in conjugation of the tricyclic aromatic system (see Scheme 1). LC is not enzymatically synthesized directly, but its biological precursor riboflavin (N10-ribityl-7,8-dimethylisoalloxazine or RBF) is biosynthesized in copious amounts by plants and bacteria using RBF synthase.[1] Animals lack the RBF synthase enzyme and must obtain RBF by ingestion.[2] Lumichrome is one of the primary products of the facile photodegradation of riboflavin and its derivatives flavin mononucleotide (FMN) and flavin adenine dinucleotide (FAD).[3,4] Additionally, LC is a product of the enzymatic catabolic degradation of riboflavin.[5]

While FAD and FMN are critical enzymatic cofactors due to their favorable reduction potentials in both ground and electronic excited states[6,7] for performing electron-transfer mediated reactions, lumichrome has not (yet) been found in this role. Its ground state reduction potential, which has only recently been determined by cyclic voltammetry, is significantly more negative than oxidized RBF[8] and more negative than most biological redox cofactors in the ground state, including nicotinamide cofactors.[9] This suggests a rationale for it not being found as a redox cofactor.

The facile photodegradation of oxidized vitamin B_2 and its derivatives efficiently produces lumichrome with the concomitant loss of the ribityl side chain, probably through a triplet-induced electron-transfer reaction.[4,10] Since flavins are ubiquitous in cellular biochemistry,[7] LC can build up in the cell with a variety of physiological consequences, principally that of a feedback regulator of riboflavin synthesis or catabolism, which proceeds via riboflavin hydrolase,[5,11–13] an enzyme that has been known since the 1940s.[14]

Another recent discovery is that lumichrome inhibits riboflavin transport in rat[15–18] and human[15,19–21] retina, possibly leading to riboflavin deficiency and ocular issues.[16,20–22] Studies on the human retina have shown similar results.[23] Lumichrome's apparent deleterious effects on cellular function render lumichrome transport essential. For this purpose, the RBF transport protein dodecin also binds LC with high affinity, presumably

for cellular waste disposal.[24] Coincidentally, the wide adoption of white light-emitting diode (LED) lamps with significant blue intensity appears to have accelerated the rate of RBF/FMN photodegradation and concomitant increase in LC formation in the retina.[25] Also of potential consequence is the use of blue light LEDs for treating seasonal affective disorders and jetlag.[26–28]

FMN is utilized as a genetically encoded singlet oxygen generator (SOG) in miniSOG proteins, parts of LOV domains[6,29,30] in which a molecule of FMN absorbs blue light to generate $^1O_2$ with high yield. The inevitable photodegradation of the FMN to LC gives a LC-miniSOG with a singlet O_2 yield an order of magnitude larger than for FMN-miniSOG, given LC's high intersystem crossing rate.[31]

LC functions as a signaling molecule. In concert with RBF, it can affect plant growth at the nanomolar level in a species-dependent manner.[32] When LC is secreted outside of the cell, it appears to provide a bacterial quorum sensing signal leading to biofilm formation.[33–35] Since biofilms of pathogenic organisms represent a human health risk, their early detection would be an important achievement. LC exhibits low fluorescence emission,[36,37] which is advantageous for second-harmonic generation (SHG) detection.

Since secretion of LC would require passage through the cell membrane, interface-sensitive stand-off spectroscopic techniques should produce sensitive optical signatures. We hypothesize that lumichrome has a sufficiently large difference dipole moment, $\mathbf{\Delta}\vec{\mu}_{fi} = \vec{\mu}_f - \vec{\mu}_i$, to facilitate noninvasive spectroscopic stand-off detection of biofilm formation[33–35] through second-harmonic generation (SHG).[38,39] SHG efficiency requires a large β (hyperpolarizability) value, which correlates positively with the magnitude of the difference dipole moment

The only experimental data on LC charge redistribution are the molecular relaxation studies on methylated LC derivatives by Shcherbatska et al., giving the magnitude of $\mathbf{\Delta}\vec{\mu}_{10}$~1 D.[40] Here, we present low-temperature absorption and Stark spectra to determine the degree and direction of charge redistribution in the two lowest-energy bright excited electronic states of lumichrome. Density functional theory (DFT) calculations at the TD-B3LYP/6–311+G(2d,p) level of theory were used to support these assignments. The hyperpolarizability of LC was estimated relative to flavin adenine dinucleotide, a tautomeric derivative. The $\mathbf{\Delta}\vec{\mu}$ obtained here confirms the result obtained by Shcherbatska et al. and is ~30% lower than $\mathbf{\Delta}\vec{\mu}_{10}$ for flavin, suggesting that it would be a modest probe of bacterial quorum sensing by SHG. However, the charge-transfer character of higher excited transitions, we will argue, will provide for stand-off detection of biofilms.

METHODS

Preparation of Lumichrome/Ethanol Solutions.

Lumichrome (99% purity) was obtained from Acros and used without further purification. However, its purity was checked by reverse-phase C18 column chromatography using 50:50 MeOH/H_2O, which showed a single peak only (Agilent 1260 with a diode array detector). All solutions were prepared fresh in anhydrous ethanol (EtOH, Pharmco-Aaper).

Extinction coefficients for lumichrome were determined on two standard solutions made by dissolving ~22 (±0.1) mg of LC in 100 mL of neat EtOH in a volumetric flask to make a saturated solution. The stoppered solution was sonicated at 65 °C for a total of 20 min and allowed to cool to room temperature. A 1 mL sample was extracted, filtered using a 0.22 μm poly(vinylidene difluoride) (PVDF) syringe filter (Fisher), and its absorbance was measured. The remaining 99 mL cloudy solution was then filtered under vacuum using a 0.22 μm poly(tetrafluoroethylene) (PTFE) membrane filter (FGLP, Millipore) that had been preweighed. The undissolved LC on the filter was weighed after drying. This mass along with the absorbance of the 1 mL filtered sample solution gave the room-temperature extinction coefficients of the two lowest-energy optical transitions of the lumichrome in dry ethanol.

UV–Vis Spectroscopy.

Room-temperature UV–vis spectra were measured in fused silica cuvettes in pathlengths from 0.1 to 1.0 cm using either a Hewlett-Packard 8453 or 8452A Diode Array Spectrophotometer. Spectra were baseline-corrected using SpectraGryph (Friedrich Menges, http://spectroscopy.ninja). The concentrations of LC/EtOH solutions were determined based on the measured extinction coefficient for LC in EtOH from the standard solutions, as described above.

The low-temperature absorption spectrum of LC in EtOH was measured using a cuvette formed from two sapphire windows measuring 1 cm in diameter and 0.52 mm in thickness (Swiss Jewel) separated by a ceramic annulus of thickness 510 μm (Upchurch Scientific). The low-temperature spectrum was measured using our in-house constructed Stark spectrometer (see below). Contraction of the EtOH upon flash-freezing to 77 K was 20 ± 5% based on measuring the change in the height of the solution versus the frozen glass. This contraction leads to an increase in concentration by a factor of 1.25.

Stark Spectrometer and Analysis.

The Stark spectrometer has been described in detail previously.[41,42] Briefly, the output of a 300 W Xe arc lamp is focused onto a 1/8 m monochromator with a 2 nm bandpass. The monochromatic probe beam is then passed through a depolarizer followed by a Glan–Taylor polarizer to control the polarization. This probe beam is then passed through the Stark cuvette, held in a two-chambered Janis cryostat filled with liquid nitrogen. After passing through the frozen sample, the light is focused onto a Si photodiode.

The Stark cuvette is constructed from two pieces of Corning boro-aluminosilicate glass (2.54 cm × 2.54 cm × 0.7 mm) coated on one side with a transparent conductive coating of indium tin oxide (100 Ω/cm, Delta Technologies). The conductive sides of the slides are separated by Kapton spacers (25 μm thickness). These Kapton spacers leave an open space between the two conductive sides of the glass slides that can be filled with the sample solution (~40 μL). The cuvette is spring-clipped to a cold finger and lowered into the inner dewar of the cryostat. The cold finger can be rotated to control χ, the angle between the polarization of incident light and the applied electric field.

A lock-in amplifier (Stanford Research Systems SR830) was used to generate a high-fidelity, low-voltage sinusoidal AC waveform at 3.5 kHz. This was amplified 1000× using a TREK 609 amplifier to obtain upward of 3×10^5 V/cm across the 25 μm pathlength cuvette. Phase-sensitive detection was performed at the second-harmonic of the amplified AC voltage.

Low-temperature absorbance spectra were taken under the same conditions as the Stark spectra with the addition of a chopper of $\omega = \sim 1$ kHz to modulate the probe beam. The spectra at several concentrations were computed according to the Beer–Lambert Law, $A = \log(I_0/I)$, where I_0 was obtained using only ethanol.

The Stark spectra were analyzed according to eq 1, the Liptay equation[43]

$$\frac{\mathbf{\Delta}\varepsilon(\bar{\nu})}{\bar{\nu}} = \left(f_C\left|\overrightarrow{F}_{\text{ext}}\right|\right)^2\left\{A_\chi\left(\frac{\varepsilon(\bar{\nu})}{\bar{\nu}}\right) + \frac{B_\chi}{15ch}\frac{\mathrm{d}}{\mathrm{d}\bar{\nu}}\left(\frac{\varepsilon(\bar{\nu})}{\bar{\nu}}\right) + \frac{C_\chi}{30c^2h^2}\frac{\mathrm{d}^2}{\mathrm{d}\bar{\nu}^2}\left(\frac{\varepsilon(\bar{\nu})}{\bar{\nu}}\right)\right\} \quad (1)$$

where $\varepsilon(\bar{\nu})$ is the extinction as a function of wavenumber, $\overrightarrow{F}_{\text{ext}}$ is the magnitude of the external electric field in V/m, f_C is the local field correction factor, c is the speed of light, and h is Planck's constant. The change in energy-weighted extinction due to an applied electric field, $\mathbf{\Delta}\varepsilon(\bar{\nu})/\bar{\nu}$, can be described as a linear combination of the zero, first, and second derivatives of the energy-weighted extinction $\varepsilon(\bar{\nu})/\bar{\nu}$ for an immobilized, isotropically oriented sample. The zero, first, and second-derivative contributions to the Stark spectrum are weighted, respectively, by the coefficients $A\chi$, $B\chi$, and $C\chi$. These coefficients are functions of parameters characterizing charge redistribution in the molecule upon optical excitation.

The $A\chi$ coefficient is related to the polarizability and hyperpolarizability of the molecule's transition dipole moment $\overrightarrow{m}$. In most cases, the transition dipole moment polarizability and hyperpolarizability are negligible, causing the zero derivative component of the Stark spectrum to be below the limit of detection of the instrument.

$$B_\chi \approx \frac{5}{2}Tr\mathbf{\Delta}\overline{\overline{\alpha}}_{fi} + \left(3\cos^2\chi - 1\right)\left(\frac{3}{2}\overrightarrow{m}_{fi}\cdot\mathbf{\Delta}\overline{\overline{\alpha}}_{fi}\cdot\overrightarrow{m}_{fi} - \frac{1}{2}Tr\mathbf{\Delta}\overline{\overline{\alpha}}_{fi}\right) \quad (2)$$

The $B\chi$ coefficient (eq 2) is a function of the change in polarizability between ground and excited states, $\mathbf{\Delta}\overline{\overline{\alpha}}_{fi} = \mathbf{\Delta}\overline{\overline{\alpha}}_f - \overline{\overline{\alpha}}_i$, as well as the projection of the mean difference polarizability along the transition dipole moment. The difference polarizability of the molecule under the application of the external electric field causes a shift in the absorption band. Because the lock-in detects $\mathbf{\Delta}I = I(F_{\text{ext}}) - I(0)$, the shift is measured as a first derivative of the absorption line shape.

Finally, the $C\chi$ term (eq 3) reports on the change in dipole moments between ground and excited states, $\mathbf{\Delta}\overrightarrow{\mu}_{fi} = \overrightarrow{\mu}_f - \overrightarrow{\mu}_i$, as well as the angle ζ_{fi} between $\overrightarrow{m}$ and $\mathbf{\Delta}\overrightarrow{\mu}$

$$C_\chi = \left|\mathbf{\Delta}\overrightarrow{\mu}_{fi}\right|^2\left\{5 + \left(3\cos^2\chi - 1\right)\left(3\cos^2\zeta_{fi} - 1\right)\right\} \quad (3)$$

The applied field leads to a broadening of the absorption spectrum and is measured as a second-derivative line shape.

Stark and low-temperature absorption spectra were fitted in the following manner. The number of electronic transitions was estimated by the electrodichroism in the Stark spectra (see below). An initial fit of the 77 K absorption spectrum was performed with 3–8 Gaussian functions per transition, and the fewest number of Gaussians that gave a fit with random residuals was used. Gaussians are attractive for this purpose not because of any physical significance but because their derivatives can be computed analytically. The computed spectrum and its derivatives also effectively remove high-frequency noise in the measured absorption spectrum. These Gaussian parameters were used as a starting point for the simultaneous fitting of Stark and absorption spectra.

A weighted nonlinear least-squares simultaneous fit to the Stark and absorption spectra was performed using our in-house program Starkfit (https://github.com/stanleyextreme/Stark-Spectroscopy-Fitter). The weighting factor selects the relative contribution of the Stark versus absorption spectrum to the simultaneous fit and allows for different S/N ratios between Stark and absorption spectra to be considered. Once the fit converges, the final parameters are fed into a Monte Carlo routine that tests the sensitivity of the fit to the value of each fitted parameter. These simulations estimate uncertainties for the fitted parameters. The analysis takes into account pathlength and angle of incidence changes due to the solvent.

Computational Methods.

All theoretical calculations were completed in the gas phase at the B3LYP/6–311+G(2d,p) level of theory using Gaussian16.[44] First, the ground state molecular geometry of lumichrome was optimized, and a frequency calculation was conducted to verify that the optimized geometry was a minimum of the nuclear potential energy surface. Second, an excited state calculation was completed to determine the transition energies, transition dipole moments, and oscillator strengths of transitions between the 10 lowest-energy electronic excited states of lumichrome. Third, the finite field method[45] was used to determine the difference permanent dipole moments characterizing electronic transitions from the ground state of lumichrome to each of the two lowest-energy electronic excited states of lumichrome of experimentally measurable oscillator strength. Briefly, the energy of a molecule in an external electric field, $E(\vec{F})$, may be approximated using a Taylor series truncated at the second term such that $E(\vec{F}) = E(0) - \vec{\mu} \cdot \vec{F}$, where $\vec{\mu}$ is the molecule's permanent dipole moment. Expanding the dot product as $\vec{\mu} \cdot \vec{F} = \left|\vec{\mu}_x\right|\left|\vec{F}_x\right| + \left|\vec{\mu}_y\right|\left|\vec{F}_y\right| + \left|\vec{\mu}_z\right|\left|\vec{F}_z\right|$ and assuming that molecular energy depends linearly on field magnitude for field magnitudes on the order of 0.001 au (~5142 V/cm), the component $\vec{\mu}$ of the permanent dipole moment may be computed as $\mu_i = -\left(\frac{E(F_i = +0.001\,\text{au}) - E(F_i = -0.001\,\text{au})}{0.002\,\text{au}}\right)$. Gaussian16 permits single-point calculations and excited state calculations to be completed with finite electric fields projected in the positive or negative direction along each of the three Cartesian axes. By cycling through

each of the six possible finite field components one at a time and computing molecular energies for the electronic ground state and the electronic excited states in the presence of each finite field, it is possible to determine the components of the permanent dipole moments of each electronic state and also therefore the components of the difference permanent dipole moment characterizing each electronic transition. Having calculated the difference dipole moment and the transition dipole moment characterizing each transition, it was possible to compute the angle between the difference dipole moment and transition dipole moment, ζ_{fi}. Difference electron densities were computed using Gaussian16 and visualized at an isovalue of 0.0025 e/au^3 using GaussView 6.0.[46] All calculations conducted for lumichrome were repeated for lumiflavin (LF).

RESULTS AND DISCUSSION

Room-temperature and low-temperature absorption spectra were obtained as described above. The 298 K spectrum (Figure 1) shows two near-UV broad bands centered at 338 and 385 nm. Based on a replicate pair of measurements, these bands have peak extinction coefficients of ε_{385nm} = 9100 ± 100 M^{-1} cm^{-1} and ε_{338nm} = 9500 ± 100 M^{-1} cm^{-1}.

There are a variety of measurements for the extinction coefficient of LC in ethanol, varying from about 4600 to 50 000 M^{-1} cm^{-1}.[3,37,47,48] The room-temperature absorption spectrum of lumichrome in dry ethanol was acquired at a range of different lumichrome concentrations up to ~1 mM, but no evidence of dimerization was observed (data not shown).

Three separate 77 K absorption spectra of LC in anhydrous ethanol were averaged (Figure 1). At 77 K, the 385 nm band shifts by +2 nm to 387 nm and becomes more structured, with apparent vibronic structure at 369 and 405 nm. The extinction falls to ε_{387nm} = 8500 ± 100 M^{-1} cm^{-1}. The band centered at 338 nm narrows and shifts +6 nm to 344 nm, with a decreased extinction coefficient of ε_{344nm} = 8000 ± 100 M^{-1} cm^{-1}.

Stark Spectra.

High signal/noise ratio Stark spectra were obtained at χ = 55 and 90° (Figure 2, data points with error bars). The electrodichroism of the Stark spectra (change in $\Delta\varepsilon$ vs χ) was examined to determine the minimum number of electronic transitions spanning the wavelength region of interest (~312–476 nm). The differing electrodichroism at approximately 340 and 380 nm strongly suggests that two electronic transitions span this range.

To verify that two electronic transitions are present, an initial absorption spectrum fit using one set of gaussians (a single transition) was performed for LC where the number of gaussians used was varied from 3 to 8. The fits were poor (fits not shown), verifying that at least two electronic transitions form the optical absorption spectrum of LC in dry ethanol.

Fits using two and three electronic transitions were then performed. Since no improvement was obtained in going from two to three transitions, the absorption/Stark spectra were fitted

under the assumption that lumichrome in dry ethanol undergoes two distinct electronic transitions in the spectral range from 312 to 476 nm.

The best fit, with the minimal, random residuals, to both the Stark and absorption spectrum for LC in anhydrous ethanol came from the two-transition fit with 14 total Gaussians (7 per transition). From this fit (see Figure 2, solid lines), we determined the values of the Stark charge redistribution parameters based on the $A\chi$, $B\chi$, and $C\chi$ coefficients, characterizing electrodichroism of LC's two optical transitions. These parameters are compiled in Table 1. All values have been corrected for the local field correction factor, f_C, which has a value of 1.65 for LC in ethanol.

Electronic Structure Calculations.

The properties of the first 10 singlet electronic excited states S_1–S_{10} of LC and LF were computed and compared to the respective ground (S_0) states. Based on the generated electron density maps (cf. Figure 3), all of these transitions have π–π^* character. The transition energy, the oscillator strength, f_{osc}, transition and difference permanent dipole moments, m_{fi} and $\Delta\mu_{fi}$, dipole moment, $\Delta\mu_{n0}$, are compiled in Table 2 for the two lowest bright electronic transitions of LC and LF. The energies of the three lowest singlet–singlet transitions of LC are within the spectral scan range (312–476 nm) and have $f_{osc} \geq 0.001$. Based on f_{osc}, the bright (observed) transitions should be assigned as S_{10} and S_{30}. However, if the S_{20} state has a significant charge-transfer (CT) character it may appear in the Stark spectra as well as a large difference mean polarizability, $Tr\Delta\bar{\bar{\alpha}}_{fi}$. No evidence of this is found. The mean polarizability change for the two observed transitions is modest and therefore the TD-DFT results suggest that the experimental data is best modeled using $|\Delta\vec{\mu}_{n0}|$ (the second derivative of the absorption spectrum) and that the assignment as S_{10} and S_{30} is correct.

Charge redistribution (excitation difference density) maps and difference dipole vector diagrams are shown in Figure 3. The computed $\vec{m}_{n0}$ of gas phase LC and LF are given as dotted arrows. The computed difference dipole moments of LC and LF are given as solid colored arrows, while the experimental difference dipole moments of LC are given as black arrows.

As shown in the ρ-CI difference density ($\Delta\rho = \rho_n - \rho_0$) map for LC, the S_{10} transition involves a relatively even redistribution of charge with $|\Delta\vec{\mu}_{10}| = 1.88\,\mathrm{D}$, confirming the low experimental $|\Delta\vec{\mu}_{10}| = 0.97\,\mathrm{D}$, as well as a small change in difference polarizability, $Tr\Delta\bar{\bar{\alpha}}_{10}$. It can be seen that the S_{10} transition in LF involves greater concentration of $\Delta\rho$ in the conjugated diazarene group (N5-C4a-C10a-N1). On the contrary, the S_{30} transition shows transfer of charge from the pyrimidine ring to the pyrazine/xylene rings. This redistribution justifies qualitatively the change in direction and increased magnitude of the $|\Delta\vec{\mu}_{30}| = 5.37\,\mathrm{D}$, compared to that for LF where $|\Delta\vec{\mu}_{40}| = 4.32\,\mathrm{D}$.

SHG Cross-section Estimate.

The probability of second-harmonic generation by an oriented ensemble of chromophores, such as those transiting a cell membrane,[49,50] is directly proportional to the second-harmonic generation cross-section characteristic of each chromophore, σ_{SHG}, which is itself proportional to the squared magnitude of the first optical molecular hyperpolarizability,[51–54] β. Within the two-level approximation, the hyperpolarizability is[55,56]

$$\beta = \frac{3e^2}{2\hbar^3}\frac{\omega_{n0} f_{n0}\left|\Delta\vec{\mu}_{n0}\right|}{\left(\omega_{n0}^2-\omega^2\right)\left(\omega_{n0}{}^2-4\omega^2\right)} \tag{4}$$

where e is the elementary unit of charge, $\hbar$ is the reduced Planck's constant, ω_{n0} is the frequency of light exciting the chromophore from the ground (g) state to the nth excited state, f_{n0} is the oscillator strength of the transition, and $\Delta\mu_{n0}$ is the chromophore's change in permanent dipole moment upon excitation. The parameter ω is equal to the frequency of the incident light.

The product, $\omega_{n0} f_{n0}\left|\Delta\vec{\mu}_{n0}\right|$, in the numerator of this equation quantifies the molecular determinants of the hyperpolarizability and thus the probability of SHG, while the product $\left(\omega_{\vec{e}g}^2-\omega^2\right)\left(\omega_{\vec{e}g}^2-4\omega^2\right)$ in the denominator quantifies the potential for resonance enhancement of second-harmonic generation as a function of the frequency of the incident light. If we assume that separate light sources are available for maximizing the resonance enhancement of two specific transitions of two different molecules, then the relative resonance-enhanced second-harmonic generation cross sections of the two molecules are a function of only each chromophore's excitation frequency, oscillator strength, and difference dipole moment, such that

$$\begin{aligned}\frac{\sigma_{\mathrm{SHG}_i}}{\sigma_{\mathrm{SHG}_j}} &= \frac{\left|\beta_i\right|^2}{\left|\beta_j\right|^2} \cong \frac{\left|\left(\omega_{n0} f_{n0}\left|\Delta\vec{\mu}_{n0}\right|\right)_i\right|^2}{\left|\left(\omega_{n0} f_{n0}\left|\Delta\vec{\mu}_{n0}\right|\right)_j\right|^2} \\ &= \frac{\left|\left(\omega_{n0}\cdot\int_{\mathrm{band}}\frac{\epsilon(\bar{v})}{\bar{v}}\mathrm{d}\bar{v}\cdot\left|\Delta\vec{\mu}_{n0}\right|\right)_i\right|^2}{\left|\left(\omega_{n0}\cdot\int_{\mathrm{band}}\frac{\epsilon(\bar{v})}{\bar{v}}\mathrm{d}\bar{v}\cdot\left|\Delta\vec{\mu}_{n0}\right|\right)_j\right|^2}\end{aligned} \tag{5}$$

where the oscillator strength f_{n0} has been substituted by the energy-weighted integrated extinction of the transition, $\int_{\mathrm{band}}\frac{\epsilon(\bar{v})}{\bar{v}}\mathrm{d}\bar{v}$, to which it is directly proportional.[57]

Second-harmonic generation by flavin derivatives designed to maximize intramolecular charge transfer via push–pull motifs has been studied by our group[58] and others.[59,60] Second-harmonic generation by native flavins, however, has been less studied. To our knowledge, the only publication of second-harmonic generation by a native flavin is that of Rinuy, Brevet, and Girault,[61] who measured resonance-enhanced second-harmonic generation by the first optical transition of molecules of oxidized flavin adenine dinucleotide bound by glucose oxidase oriented at an air/water interface. While no Stark spectroscopic study of glucose oxidase has been completed to directly compare LC's potential for second-harmonic generation to that of FAD bound by glucose oxidase in terms of intramolecular

charge redistribution, we have published a Stark spectroscopic study of oxidized FAD bound by photolyase.[62] The cofactor binding pockets of glucose oxidase and photolyase differ structurally, but to a first approximation both are predominantly hydrophobic protein environments excluding solvent.

The first optically bright transition of oxidized FAD in photolyase is characterized by an excitation frequency of 674.49 THz (corresponding to a λ_{max} of 444.48 nm), an integrated energy-weighted extinction of 1747.37 M^{-1} cm^{-1}, and a difference dipole moment of 1.7 D. Since the first optically bright transition in LC has a smaller difference dipole (~1 D), we choose to exploit the next optically bright transition, $n = 0 \rightarrow 3$ in the TD-DFT result, for comparison with FAD, using the work on two-photon cross sections in higher excited states of trans-stilbene as a guide.[63] Th S_{30} transition of LC in ethanol is characterized by an excitation frequency of 889.98 THz (corresponding to a λ_{max} of 336.98 nm, Figure 1), an integrated energy-weighted extinction of 919.17 M^{-1} cm^{-1}, and a difference dipole moment of 2.2 D.

Assuming resonant illumination of each transition at appropriate energies, these molecular parameters indicate that the relative resonance-enhanced second-harmonic generation cross sections of these transitions of these chromophores to be

$$\frac{\sigma \mathrm{SHG}_{\mathrm{LC}}}{\sigma \mathrm{SHG}_{\mathrm{FAD}}} = \frac{|\beta_{\mathrm{LC}}|^2}{|\beta_{\mathrm{FAD}}|^2} \cong \frac{\left|\left(\omega_{n0} \cdot \int_{\mathrm{band}} \frac{\varepsilon(\nu)}{\nu} \mathrm{d}\nu \cdot |\Delta \vec{\mu}_{n0}|\right)_{\mathrm{LC}}\right|^2}{\left|\left(\omega_{n0} \cdot \int_{\mathrm{band}} \frac{\varepsilon(\nu)}{\nu} \mathrm{d}\nu \cdot |\Delta \mu_{n0}|\right)_{\mathrm{FAD}}\right|^2}$$
$$= \frac{\left|674.49\,\mathrm{THz} \cdot 1747.37\,\mathrm{M}^{-1}\,\mathrm{cm}^{-1} \cdot 1.7\mathrm{D}\right|^2}{\left|889.98\,\mathrm{THz} \cdot 919.17\,\mathrm{M}^{-1}\,\mathrm{cm}^{-1} \cdot 2.2\mathrm{D}\right|^2} = 0.81$$

The S_{10} transition of oxidized FAD bound in a protein environment is characterized by a lower energy and slightly smaller difference dipole moment than the S_{30} transition of LC but also by a significantly greater energy-weighted integrated extinction, giving $\sigma_{\mathrm{SHG}}^{\mathrm{LC}} \sim 0.8\,\sigma_{\mathrm{SHG}}^{\mathrm{FAD}}$. Because the first optically bright transition of FAD bound within a protein environment has previously been demonstrated to be robustly capable of resonance-enhanced second-harmonic generation and the resonance-enhanced second-harmonic generation cross section of the second optically bright transition of LC is just 20% less than that of FAD's first transition, we conclude that LC should function as an experimentally viable intramembrane second-harmonic generation probe.

Here, we have presented the room-temperature absorption, low-temperature absorption, and Stark spectra for lumichrome in dry ethanol. Since flavin has a useful SHG cross section, we hypothesized that LC might also be a useful nonlinear spectroscopic probe of bacterial quorum sensing, an indicator of retinal health, or in any situation where LC is used as a signaling molecule through an interface as well. Since RBF and FMN must pass through membranes, we speculated that LC, in particular, would also be a good SHG probe of riboflavin/FMN uptake, transport, and photodegradation. Excitation of LC can be accomplished using Ti:sapphire oscillators from 750 to 840 nm, a range at which light has a large tissue penetration depth. A further advantage of LC for SHG stand-off detection is

its intrinsically small emission quantum yield. For FMN and RBF with (λ_{em}^{max}~530 nm), $\Phi_F \approx 0.25$,[64,65] but $\Phi_F \approx 0.04$ for LC (λ_{em}^{max}~480 nm).[4] However, for SHG detection, fluorescence is an interfering background component, so the low Φ_F for LC is an ~6-fold lowering of this background.

To conclude, LC is collected and secreted from the cell as a waste product from photodegradation and catabolism of cellular flavins, so that it is not surprising that it is found to act as a biochemical signal for quorum sensing.[34] An interesting opportunity exists for LC imaging at interfaces by SHG, since it is used in quorum sensing and thus must be transported through the cell membrane, since the secretion process will involve LC at interfaces it may be a useful indicator of metabolic stress and biofilm proliferation. A final determination of its usefulness as a SHG probe in these cases awaits dedicated experimentation.

Supplementary Material

Refer to Web version on PubMed Central for supplementary material.

ACKNOWLEDGMENTS

This manuscript is dedicated to Professor Hai-Lung Dai, whose leadership and creativity in chemical research is inspirational. Steven E. Meckel, a former M.S. student in the group, performed useful Stark spectroscopic measurements on hydrated lumichrome that did not appear in this manuscript. We are very grateful to Dr. Spiridoula Matsika and Dr. Vincent Spata for initial calculations and useful discussions. The authors made the following contributions to this work: D.T.B. collected and analyzed low-temperature absorption and Stark spectra on LC in water-containing ethanol. They (and R.J.S.) were supported in part by a grant from NASA (NNX13AH33G). C.v.G. collected room- and low-temperature absorption and 77 K Stark spectra on LC in dry ethanol, analyzed these data, performed the quantum mechanical calculations, and was a writer of the manuscript. C.v.G and R.J.S. designed the experiments and co-wrote the manuscript. They were supported in part by a grant from NASA (80NSSC17K0033).

REFERENCES

(1). Bacher A; Eberhardt S; Fischer M; Mortl S; Kis K; Kugelbrey K; Scheuring J; Schott K Biosynthesis of Riboflavin: Lumazine Synthase and Riboflavin Synthase. Methods Enzymol. 1997, 280, 389–399. [PubMed: 9211334]

(2). Abbas CA; Sibirny AA Genetic Control of Biosynthesis and Transport of Riboflavin and Flavin Nucleotides and Construction of Robust Biotechnological Producers. Microbiol. Mol. Biol. Rev 2011, 75, 321–360. [PubMed: 21646432]

(3). Koziol J Studies on Flavins in Organic Solvents-I.* Spectral Characteristics of Riboflavin, Riboflavin Tetrabutyrate and Lumichrome. Photochem. Photobiol 1966, 5, 41–54.

(4). Holzer W; Shirdel J; Zirak P; Penzkofer A; Hegemann P; Deutzmann R; Hochmuth E Photo-Induced Degradation of Some Flavins in Aqueous Solution. Chem. Phys 2005, 308, 69–78.

(5). Xu H; Chakrabarty Y; Philmus B; Mehta AP; Bhandari D; Hohmann HP; Begley TP Identification of the First Riboflavin Catabolic Gene Cluster Isolated from *Microbacterium maritypicum* G10. J. Biol. Chem 2016, 291, 23506–23515. [PubMed: 27590337]

(6). Losi A Flavin-Based Blue-Light Photosensors: A Photobiophysics Update. Photochem. Photobiol 2007, 83, 1283–1300. [PubMed: 18028200]

(7). Macheroux P; Kappes B; Ealick SE Flavogenomics - a Genomic and Structural View of Flavin-Dependent Proteins. FEBS J. 2011, 278, 2625–2634. [PubMed: 21635694]

(8). Hong J; Lee M; Lee B; Seo DH; Park CB; Kang K Biologically Inspired Pteridine Redox Centres for Rechargeable Batteries. Nat. Commun 2014, 5, No. 742.

(9). Nelson DL; Cox MM Lehninger Principles of Biochemistry; Freeman WH: New York, 2017.

(10). Song SH; Dick B; Penzkofer A Photo-Induced Reduction of Flavin Mononucleotide in Aqueous Solutions. Chem. Phys 2007, 332, 55–65.

(11). Giancaspero TA; Busco G; Panebianco C; Carmone C; Miccolis A; Liuzzi GM; Colella M; Barile M Fad Synthesis and Degradation in the Nucleus Create a Local Flavin Cofactor Pool. J. Biol. Chem 2013, 288, 29069–29080. [PubMed: 23946482]

(12). Maruta T; Yoshimoto T; Ito D; Ogawa T; Tamoi M; Yoshimura K; Shigeoka S An Arabidopsis Fad Pyrophosphohydrolase, Atnudx23, Is Involved in Flavin Homeostasis. Plant Cell Physiol. 2012, 53, 1106–1116. [PubMed: 22505691]

(13). Yanagita T; Foster JW Bacterial Riboflavin Hydrolase. J. Biol. Chem 1956, 221, 593–607. [PubMed: 13357454]

(14). Foster JW Microbiological Aspects of Riboflavin I Introduction Ii Bacterial Oxidation of Riboflavin to Lumichrome. J. Bacteriol 1944, 47, 27–41. [PubMed: 16560748]

(15). Kelley RA; Al-Ubaidi MR; Sinha T; Genc AM; Makia MS; Ikelle L; Naash MI Ablation of the Riboflavin-Binding Protein Retbindin Reduces Flavin Levels and Leads to Progressive and Dose-Dependent Degeneration of Rods and Cones. J. Biol. Chem 2017, 292, 21023–21034. [PubMed: 29079576]

(16). Kubo Y; Yahata S; Miki S; Akanuma S; Hosoya K Blood-to-Retina Transport of Riboflavin Via Rfvts at the Inner Blood-Retinal Barrier. Drug Metab. Pharmacokinet 2017, 32, 92–99. [PubMed: 27964953]

(17). Batey DW; Eckhert CD Analysis of Flavins in Ocular-Tissues of the Rabbit. Invest. Ophthalmol. Visual Sci 1991, 32, 1981–1985.

(18). Santamaria L; Latte B; Calendi E; Masala B Action Spectra of the Photodynamic Sensitivity of the Retina. Boll. Chim. Farm 1971, 110, 312–316. [PubMed: 5110578]

(19). Kansara V; Pal D; Jain R; Mitra AK Identification and Functional Characterization of Riboflavin Transporter in Human-Derived Retinoblastoma Cell Line (Y-79): Mechanisms of Cellular Uptake and Translocation. J. Ocul. Pharmacol. Ther 2005, 21, 275–287. [PubMed: 16117691]

(20). Said HM; Wang SL; Ma TY Mechanism of Riboflavin Uptake by Cultured Human Retinal Pigment Epithelial Arpe-19 Cells: Possible Regulation by an Intracellular Ca2+-Calmodulin-Mediated Pathway. J. Physiol 2005, 566, 369–377. [PubMed: 15878949]

(21). Kelley RA; Al-Ubaidi MR; Naash MI Retbindin Is an Extracellular Riboflavin-Binding Protein Found at the Photoreceptor/Retinal Pigment Epithelium Interface. J. Biol. Chem 2015, 290, 5041–5052. [PubMed: 25542898]

(22). Kubo Y; Akanuma S; Hosoya K Recent Advances in Drug and Nutrient Transport across the Blood-Retinal Barrier. Expert Opin. Drug Metab. Toxicol 2018, 14, 513–531. [PubMed: 29719158]

(23). D'Amico Donald J; Masonson HN; Patel M; Adamis AP; Cunningham ET, Jr; Guyer, D. R.; Katz, B. Pegaptanib Sodium for Neovascular Age-Related Macular Degeneration: Two-Year Safety Results of the Two Prospective, Multicenter, Controlled Clinical Trials. Ophthalmology 2006, 113, 992.e6–1001.e6. [PubMed: 16647134]

(24). Grininger M; Zeth K; Oesterhelt D Dodecins: A Family of Lumichrome Binding Proteins. J. Mol. Biol 2006, 357, 842–857. [PubMed: 16460756]

(25). Jaadane I; Rodriguez GEV; Boulenguez P; Chahory S; Carre S; Savoldelli M; Jonet L; Behar-Cohen F; Martinsons C; Torriglia A Effects of White Light-Emitting Diode (Led) Exposure on Retinal Pigment Epithelium in Vivo. J. Cell. Mol. Med 2017, 21, 3453–3466. [PubMed: 28661040]

(26). Rosenthal NE; Sack DA; Gillin JC; Lewy AJ; Goodwin FK; Davenport Y; Mueller PS; Newsome DA; Wehr TA Seasonal Affective-Disorder - a Description of the Syndrome and Preliminary Findings with Light Therapy. Arch. Gen. Psychiatry 1984, 41, 72–80. [PubMed: 6581756]

(27). Bonmati-Carrion MA; Arguelles-Prieto R; Martinez-Madrid MJ; Reiter R; Hardeland R; Rol MA; Madrid JA Protecting the Melatonin Rhythm through Circadian Healthy Light Exposure. Int. J. Mol. Sci 2014, 15, 23448–23500. [PubMed: 25526564]

(28). Stephenson KM; Schroder CM; Bertschy G; Bourgin P Complex Interaction of Circadian and Non-Circadian Effects of Light on Mood: Shedding New Light on an Old Story. Sleep Med. Rev 2012, 16, 445–454. [PubMed: 22244990]

(29). Kennis JTM; Crosson S; Gauden M; van Stokkum IHM; Moffat K; van Grondelle R Primary Reactions of the Lov2 Domain of Phototropin, a Plant Blue-Light Photoreceptor. Biochemistry 2003, 42, 3385–3392. [PubMed: 12653541]

(30). Swartz TE; Corchnoy SB; Christie JM; Lewis JW; Szundi I; Briggs WR; Bogomolni RA The Photocycle of a Flavin-Binding Domain of the Blue Light Photoreceptor Phototropin. J. Biol. Chem 2001, 276, 36493–36500. [PubMed: 11443119]

(31). Torra J; Lafaye C; Signor L; Aumonier S; Flors C; Shu XK; Nonell S; Gotthard G; Royant A Tailing Minisog: Structural Bases of the Complex Photophysics of a Flavin-Binding Singlet Oxygen Photosensitizing Protein. Sci. Rep 2019, 9, No. e10001041.

(32). Dakora FD; Matiru VN; Kanu A Rhizosphere Ecology of Lumichrome and Riboflavin, Two Bacterial Signal Molecules Eliciting Developmental Changes in Plants. Front. Plant Sci 2015, 6, No. 1505.

(33). Mattmann ME; Blackwell HE Small Molecules That Modulate Quorum Sensing and Control Virulence in *Pseudomonas aeruginosa*. J. Org. Chem 2010, 75, 6737–6746. [PubMed: 20672805]

(34). Rajamani S; Bauer WD; Robinson JB; Farrow JM; Pesci EC; Teplitski M; Gao MS; Sayre RT; Phillips DA The Vitamin Riboflavin and Its Derivative Lumichrome Activate the Lasr Bacterial Quorum-Sensing Receptor. Mol. Plant-Microbe Interact 2008, 21, 1184–1192. [PubMed: 18700823]

(35). Cooper JE Early Interactions between Legumes and Rhizobia: Disclosing Complexity in a Molecular Dialogue. J. Appl. Microbiol 2007, 103, 1355–1365. [PubMed: 17953546]

(36). Song P-S; Choi JD Fluorescence of Phototautomeric Lumichrome in Pyridine-Dioxane. Bull. Korean Chem. Soc 1980, 1, 93–97.

(37). Moyon NS; Mitra S Fluorescence Solvatochromism in Lumichrome and Excited-State Tautomerization: A Combined Experimental and Dft Study. J. Phys. Chem. A 2011, 115, 2456–2464. [PubMed: 21388154]

(38). Sharifian Gh M; Wilhelm MJ; Moore M; Dai HL Spatially Resolved Membrane Transport in a Single Cell Imaged by Second Harmonic Light Scattering. Biochemistry 2019, 58, 1841–1844. [PubMed: 30912648]

(39). Sharifian Gh M; Wilhelm MJ; Dai HL Azithromycin-Lnduced Changes to Bacterial Membrane Properties Monitored in Vitro by Second-Harmonic Light Scattering. ACS Med. Chem. Lett 2018, 9, 569–574. [PubMed: 29937984]

(40). Shcherbatska NV; van Hoek A; Visser AJWG; Koziol J Molecular Relaxation Spectroscopy of Lumichrome. J. Photochem. Photobiol., A 1994, 78, 241–246.

(41). Stanley RJ; van Galen CJ Measuring Electronic Structure Properties of Flavins and Flavoproteins by Electronic Stark Spectroscopy. In Methods in Enzymology; Palfey BA, Ed.; Elsevier, 2019; Vol. 620, pp 215–250. [PubMed: 31072488]

(42). Pauszek RF; Stanley RJA “How-to” Guide to the Stark Spectroscopy of Flavins and Flavoproteins. In Flavins and Flavoproteins: Methods and Protocols; Weber S; Schleicher E, Eds.; 2014; Vol. 1146, pp 443–466.

(43). Liptay W Dipole Moments and Polarizabilities of Molecules in Excited Electronic States. In Excited States; Lim EC, Ed.; Academic Press, Inc.: New York, 1974; Vol. 1, pp 129–229.

(44). Frisch MJ; Trucks GW; Schlegel HB; Scuseria GE; Robb MA; Cheeseman JR; Scalmani G; Barone V; Petersson GA; Nakatsuji H et al..et al.Gaussian 16, revision C.01; Gaussian 16: Wallingford, CT, 2016.

(45). Locknar SA; Peteanu LA; Shuai Z Calculation of Ground and Excited State Polarizabilities of Unsubstituted and Donor/Acceptor Polyenes: A Comparison of the Finite-Field and Sum-over-States Methods. J. Phys. Chem. A 1999, 103, 2197–2201.

(46). Dennington R; Keith TA; Millam JM Gaussview 6. Semichem Inc.: Shawnee Mission, KS, 2016.

(47). Sikorska E; Sikorski M; Steer RP; Wilkinson F; Worrall DR Efficiency of Singlet Oxygen Generation by Alloxazines and Isoalloxazines. J. Chem. Soc., Faraday Trans 1998, 94, 2347–2353.

(48). Penzkofer A Absorption and Emission Spectroscopic Investigation of Alloxazine in Aqueous Solutions and Comparison with Lumichrome. J. Photochem. Photobiol., A 2016, 314, 114–124.

(49). Zeng J; Eckenrode HM; Dounce SM; Dai HL Time-Resolved Molecular Transport across Living Cell Membranes. Biophys. J 2013, 104, 139–145. [PubMed: 23332066]

(50). Moreaux L; Sandre O; Mertz J Membrane Imaging by Second-Harmonic Generation Microscopy. J. Opt. Soc. Am. B 2000, 17, 1685–1694.

(51). Oudar JL Optical Nonlinearities of Conjugated Molecules - Stilbene Derivatives and Highly Polar Aromatic-Compounds. J. Chem. Phys 1977, 67, 446–457.

(52). Karki L; Vance FW; Hupp JT; LeCours SM; Therien MJ Electronic Stark Effect Studies of a Porphyrin-Based Push-Pull Chromophore Displaying a Large First Hyperpolarizability: State-Specific Contributions to Beta. J. Am. Chem. Soc 1998, 120, 2606–2611.

(53). Willetts A; Rice JE; Burland DM; Shelton DP Problems in the Comparison of Theoretical and Experimental Hyperpolarizabilities. J. Chem. Phys 1992, 97, 7590–7599.

(54). Marder SR; Beratan DN; Cheng LT Approaches for Optimizing the 1st Electronic Hyperpolarizability of Conjugated Organic-Molecules. Science 1991, 252, 103–106. [PubMed: 17739081]

(55). Campagnola PJ; Wei MD; Lewis A; Loew LM High-Resolution Nonlinear Optical Imaging of Live Cells by Second Harmonic Generation. Biophys. J 1999, 77, 3341–3349. [PubMed: 10585956]

(56). Albert IDL; Marks TJ; Ratner MA Remarkable Nlo Response and Infrared Absorption in Simple Twisted Molecular Pi-Chromophores. J. Am. Chem. Soc 1998, 120, 11174–11181.

(57). McHale JL Molecular Spectroscopy; Prentice-Hall: Upper Saddle River, NJ, 1999.

(58). Pauszek RF; Kodali G; Caldwell ST; Fitzpatrick B; Zainalabdeen NY; Cooke G; Rotello VM; Stanley RJ Excited State Charge Redistribution and Dynamics in the Donor-Pi-Acceptor Flavin Derivative Abfl. J. Phys. Chem. B 2013, 117, 15684–15694. [PubMed: 24020957]

(59). Mohammed N; Wiles AA; Belsley M; Fernandes SSM; Cariello M; Rotello VM; Raposo MMM; Cooke G Synthesis and Characterisation of Push-Pull Flavin Dyes with Efficient Second Harmonic Generation (Shg) Properties. RSC Adv. 2017, 7, 24462–24469.

(60). Richtar J; Heinrichova P; Apaydin DH; Schmiedova V; Yumusak C; Kovalenko A; Weiter M; Sariciftci NS; Krajcovic J Novel Riboflavin-Inspired Conjugated Bio-Organic Semiconductors. Molecules 2018, 23, No. 2271.

(61). Rinuy J; Brevet PF; Girault HH Second Harmonic Generation of Glucose Oxidase at the Air/Water Interface. Biophys. J 1999, 77, 3350–3355. [PubMed: 10585957]

(62). Kodali G; Siddiqui SU; Stanley RJ Charge Redistribution in Oxidized and Semiquinone E. coli DNA Photolyase Upon Photoexcitation: Stark Spectroscopy Reveals a Rationale for the Position of Trp382. J. Am. Chem. Soc 2009, 131, 4795–4807. [PubMed: 19292445]

(63). Houk AL; Zheldakov IL; Tommey TA; Elles CG Two-Photon Excitation of Trans-Stilbene: Spectroscopy and Dynamics of Electronically Excited States above S-1. J. Phys. Chem. B 2015, 119, 9335–9344. [PubMed: 25369524]

(64). Weber G Fluorescence of Riboflavin and Flavin-Adenine Dinucleotide. Biochem. J 1950, 47, 114–121. [PubMed: 14791317]

(65). Barrio JR; Tolman GL; Leonard NJ; Spencer RD; Weber G Flavin 1, N6-Ethenoadenine Dinucleotide: Dynamic and Static Quenching of Fluorescence. Proc. Natl. Acad. Sci. U.S.A 1973, 70, 941–943. [PubMed: 4515004]

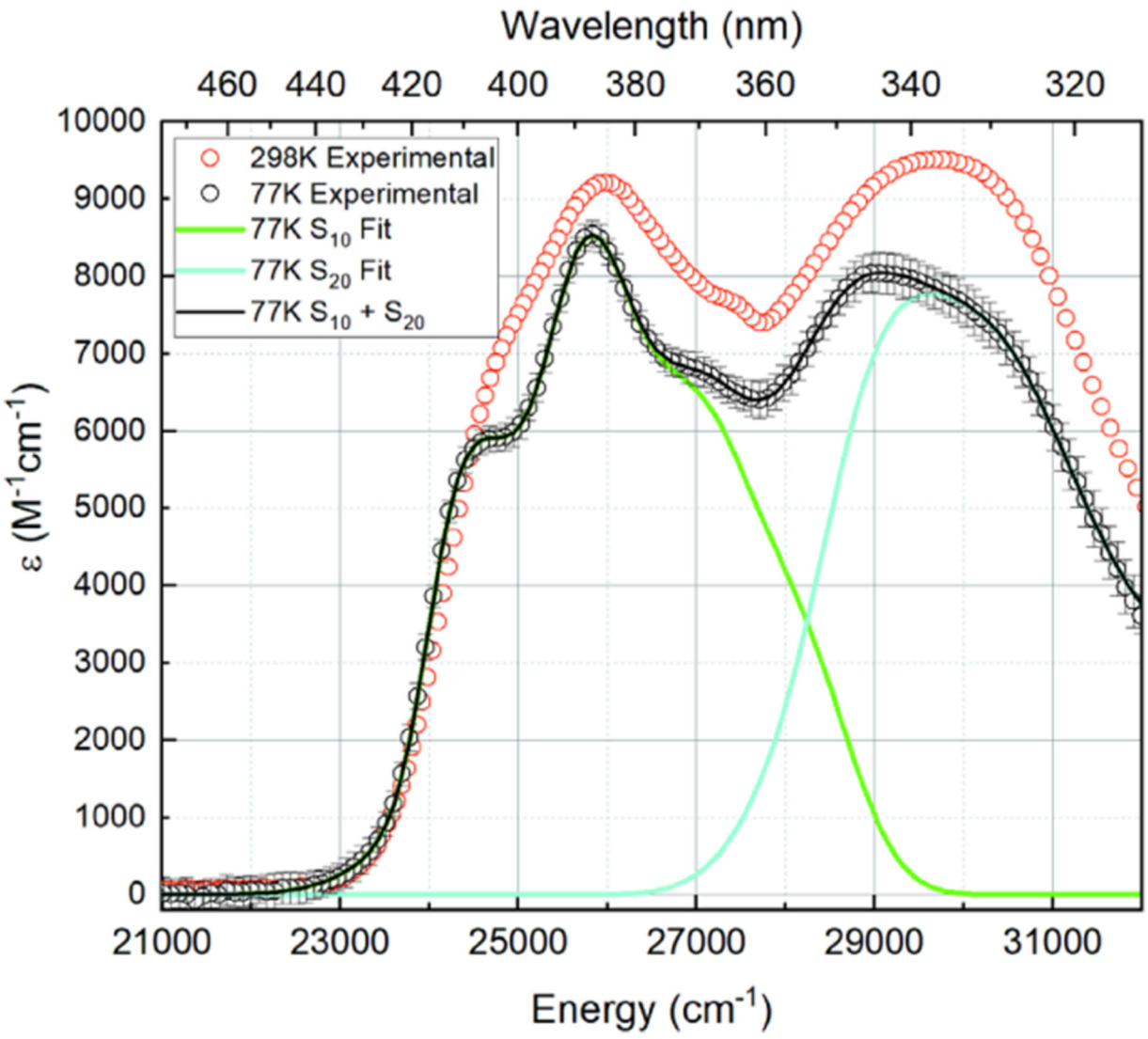

Figure 1.

298 K (red circle open) and 77 K (○) absorption spectra of lumichrome in dry ethanol, with transition-specific (green/cyan lines) and total fit (black line) to the 77 K absorption spectrum.

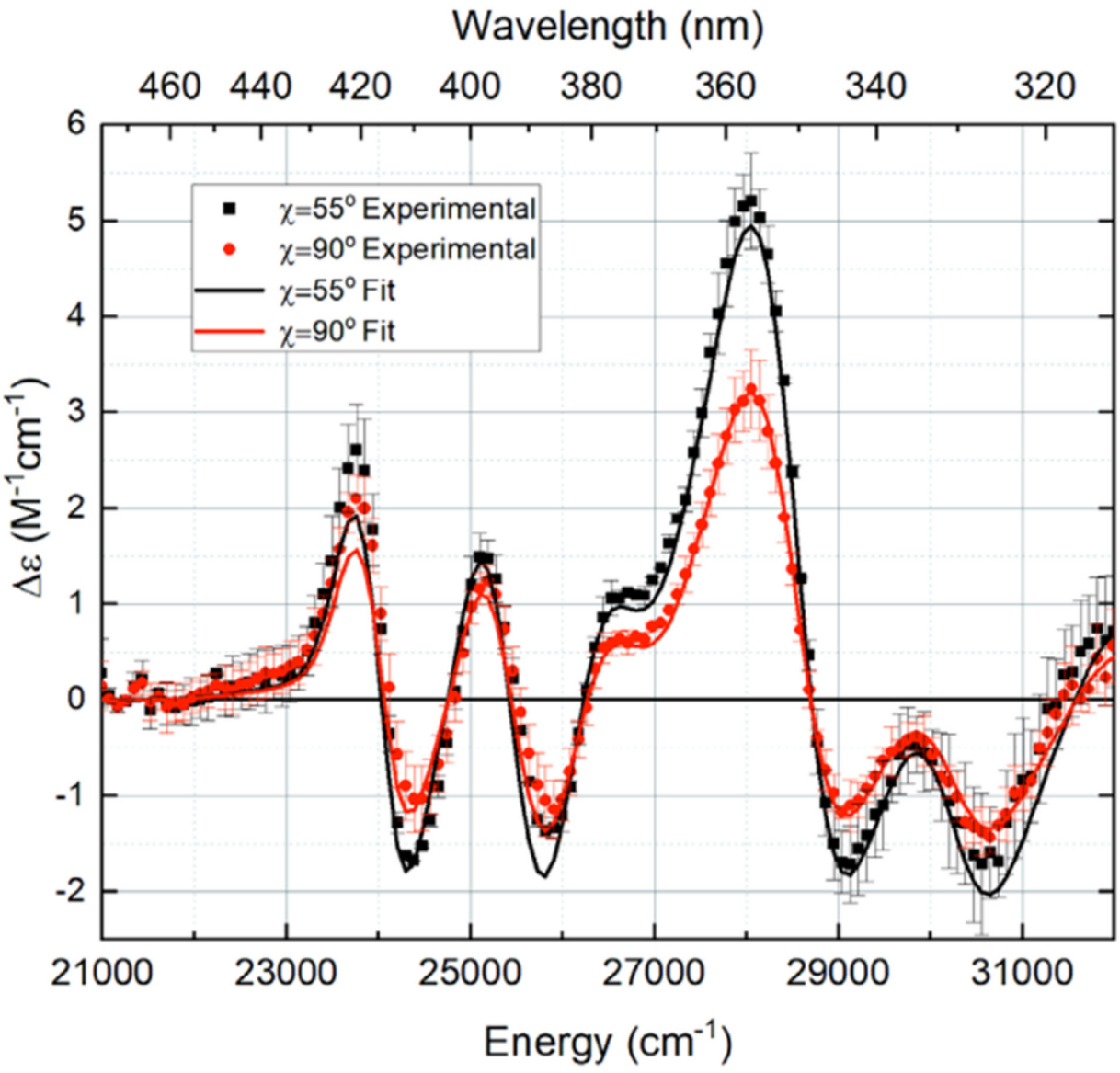

Figure 2.

LC Stark spectra at two χ angles, normalized to an applied external field of 1 MV/cm. The χ = 55° results are an average of two spectra averaged over 10 scans each, and the χ = 90° results are an average of three such spectra. Representative error bars are one standard deviation from the mean.

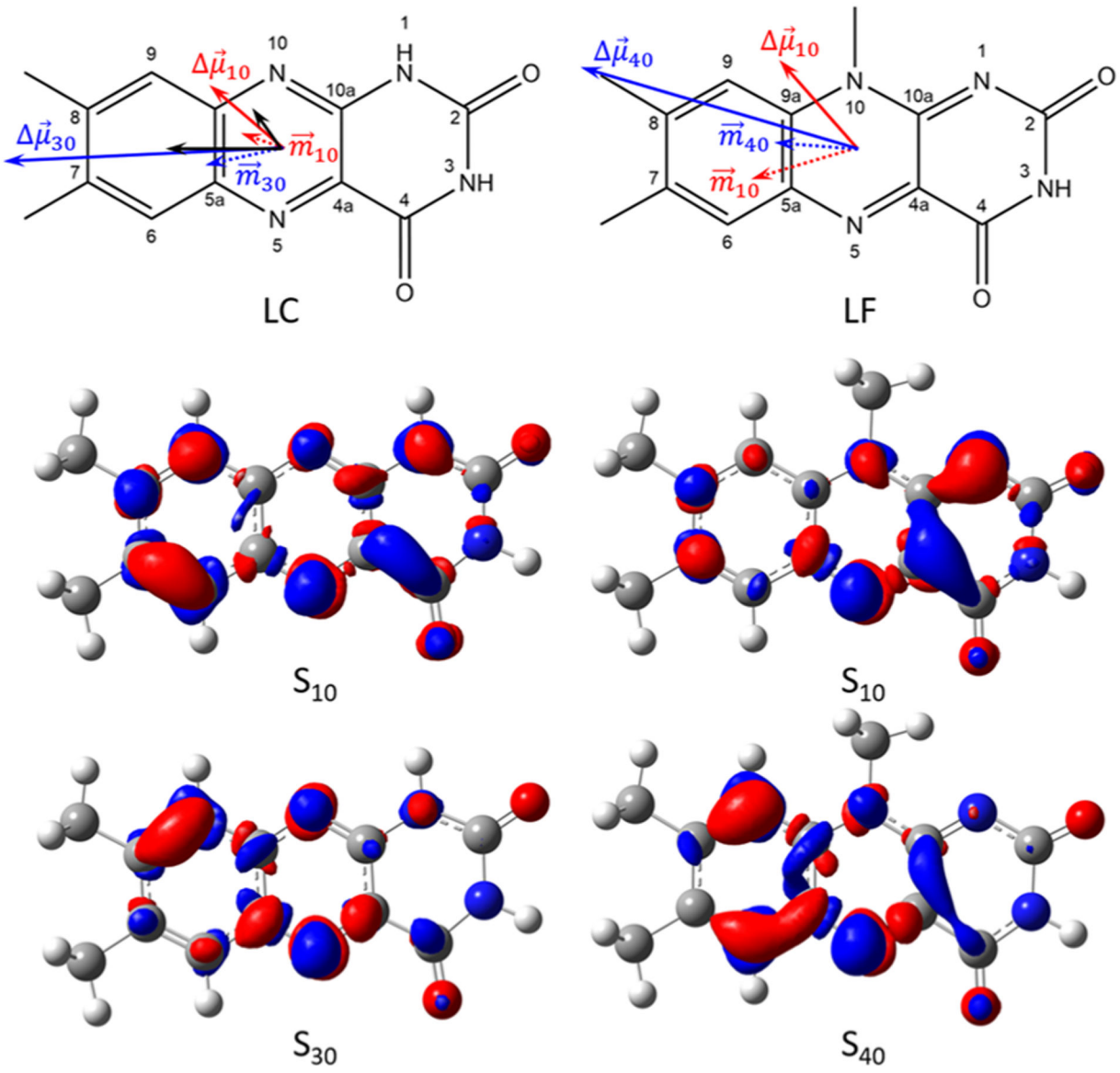

Figure 3.

Top: Calculated difference dipole moments for unsolvated lumichrome and lumiflavin calculated at the B3LYP/6–311+G(2d,p) level of theory. Bottom: Difference density maps of LC and LF. The isovalue used is 0.0025 e^{-}/au^{3}. Red is an increase in electron density, while blue indicates a decreased electron density on excitation. Modest charge redistribution occurs for the S_{10} transition, but for higher excitations charge moves from the pyrimidine to the xylene ring.

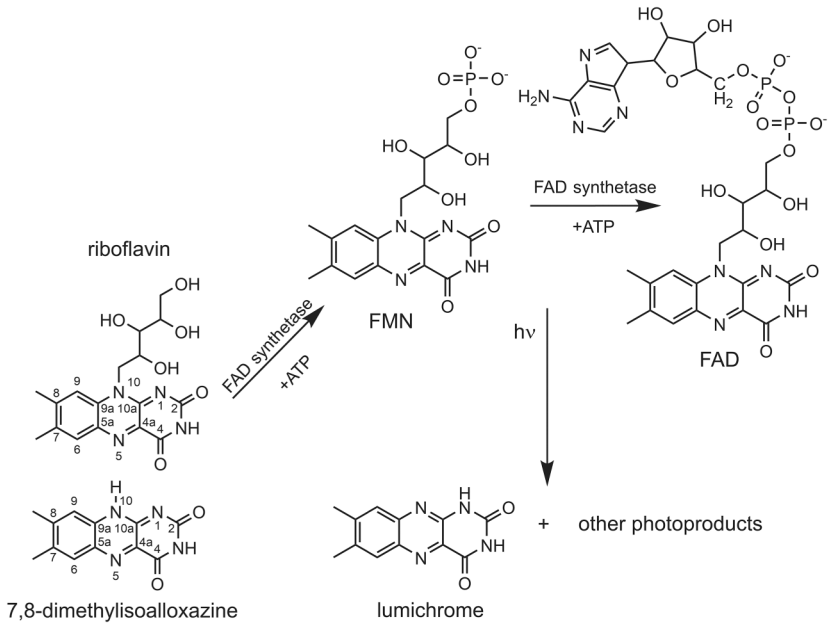

Scheme 1.

Lumichrome and Other Degradation Products are Generated from Riboflavin, FMN, and FAD through Photodegradation and Catabolism of Riboflavin by the Enzyme RcaE in Bacteria

Table 1.

Fit Charge Redistribution Parameters for LC in Dry Ethanol at 77 K[a]

transition	λ_{max} (nm)	ε_{max} (M^{-1} cm^{-1})	$Tr\Delta\bar{\bar{\alpha}}_{fi}\left(Å^3\right)$	$\vec{m}_{fi}\cdot\Delta\bar{\bar{\alpha}}_{fi}\cdot\vec{m}_{fi}\left(D^2\cdot Å^3\right)$	$\lvert\Delta\vec{\mu}_{fi}\rvert$(D)	ς_A (deg)
S_{10}	387 ± 2	8500 ± 100	5.9 ± 0.6	1.1 ± 0.6	0.97 ± 0.03	30 ± 11
S_{30}	344 ± 2	8000 ± 100	38 ± 3	28 ± 4	2.2 ± 0.1	23 ± 9

[a]Transitions are assigned on the basis of time-dependent DFT (TD-DFT) calculations.

Table 2.

TD-DFT Results for Lumichrome and Lumiflavin in Vacuo

compound	transition	λ (nm)	f_{osc}	$\lvert\vec{m}_{fi}\rvert$(D)	$\lvert\Delta\vec{\mu}_{fi}\rvert$ (D)	ς_A (deg)
Iumichrome	S_{10}	367.00	0.0649	0.8792	1.8840	21.05
	S_{30}	321.84	0.2235	1.5344	5.3658	17.21
lumiflavin	S_{10}	412.92	0.1993	1.6484	1.7674	65.33
	S_{40}	325.27	0.1464	1.2540	4.3219	11.55